Condensation and thermalization of classsical optical waves in a waveguide

P. Aschieri,[1] J. Garnier,[2] C. Michel,[3] V. Doya,[1] and A. Picozzi[3]

[1]*Laboratoire de Physique de la Matière Condensée, CNRS, University of Nice Sophia-Antipolis, F-06108 Nice, France*

[2]*Laboratoire de Probabilités et Modèles Aléatoires, University of Paris VII, F-75251 Paris, France*

[3]*Laboratoire Interdisciplinaire Carnot de Bourgogne, CNRS, University of Burgundy, F-21078 Dijon, France*

(Received 17 December 2010; published 31 March 2011)

We consider the long-term evolution of a random nonlinear wave that propagates in a multimode optical waveguide. The optical wave exhibits a thermalization process characterized by an irreversible evolution toward an equilibrium state. The tails of the equilibrium distribution satisfy the property of energy equipartition among the modes of the waveguide. As a consequence of this thermalization, the optical field undergoes a process of classical wave condensation, which is characterized by a macroscopic occupation of the fundamental mode of the waveguide. Considering the nonlinear Schrödinger equation with a confining potential, we formulate a wave turbulence description of the random wave into the basis of the eigenmodes of the waveguide. The condensate amplitude is calculated analytically as a function of the wave energy, and it is found in quantitative agreement with the numerical simulations. The analysis reveals that the waveguide configuration introduces an effective physical frequency cutoff, which regularizes the ultraviolet catastrophe inherent to the ensemble of classical nonlinear waves. The numerical simulations have been performed in the framework of a readily accessible nonlinear fiber optics experiment.

DOI: 10.1103/PhysRevA.83.033838 PACS number(s): 42.65.Sf, 42.81.Dp

I. INTRODUCTION

Statistical nonlinear optics (i.e., the study of nonlinear optics with incoherent waves) is a subject of growing interest this last decade. In particular, it has received renewed interest since the first demonstration of incoherent solitons [1–4] whose existence was theoretically predicted in the context of plasma physics [5]. More recently, incoherent nonlinear optics has also been studied in various fields of investigation, including wave propagation in homogeneous [6–9] or periodic media [10], nonlinear imaging [11], cavity systems [12–17], or nonlinear interferometry [18]. In particular, the process of *optical wave condensation* attracted some significant recent interest in different experiments realized in dissipative laser systems [12,13] and in a conservative (Kerr-like) system [19]. In this latter example, the mechanism underlying wave condensation finds its origin in the natural thermalization of the optical field toward a thermodynamic equilibrium state. Optical wave thermalization [7,8,17] is characterized by an irreversible evolution of the wave toward the "most disordered" state [i.e., the Rayleigh-Jeans (RJ) equilibrium state that realizes the maximum of entropy]. Wave turbulence (WT) theory is known to provide a detailed description of this nonequilibrium thermalization process [20–22]. In particular, it predicts the existence of a condensation process for the random nonlinear wave [23–26], whose thermodynamic properties are analogous to those of quantum Bose-Einstein condensation, in spite of the classical nature of the nonlinear wave [24,26]. More specifically, wave condensation is characterized by the spontaneous formation of a large-scale coherent structure (plane wave) starting from an initial incoherent field: The plane-wave solution ("condensate") remains immersed in a sea of small-scale fluctuations ("uncondensed quasiparticles"), which store the information necessary for the reversible evolution of the wave.

The WT description of wave condensation has been essentially developed in the ideal situation in which the random wave is supposed to be "infinitely extended in space," (i.e., its random fluctuations are assumed statistically homogeneous in space [23,24,26]). As a matter of fact, a spatially localized random optical beam experiences incoherent diffraction during its propagation, which thus inevitably affects the processes of wave thermalization and condensation. Our aim in this article is to stimulate a novel class of optical turbulence experiments in a spatial waveguide geometry. In the guided configuration, incoherent diffraction is compensated by a confining potential, thus allowing to study the thermalization and the condensation of the optical field over large propagation distances.

As a result of the guided geometry, the incoherent optical beam is confined in space and thus exhibits spatial fluctuations that are *statistically inhomogeneous*. Considering the nonlinear Schrödinger (NLS) equation with a confining potential $V(\mathbf{r})$, we formulate a WT description of the random wave into the basis of the eigenmodes of the waveguide (i.e., potential's eigenmodes), instead of the usual plane-wave Fourier basis relevant to statistically homogeneous random waves [$V(\mathbf{r}) = 0$]. The theory reveals a macroscopic occupation of the fundamental mode of the waveguide for an energy of the wave smaller than a critical value. The condensate fraction is calculated analytically as a function of the energy of the wave. It is found in quantitative agreement with the numerical simulations, without using adjustable parameters. In particular, the simulations confirm a key property of the thermalization process, namely the emergence of an equipartition of the energy among the modes of the waveguide. Furthermore, the conventional WT description of wave condensation requires the introduction of a frequency cutoff in the theory [24,26]. This regularizes the ultraviolet catastrophe inherent to classical nonlinear waves, a feature that has been analyzed in detail in the framework of the classical description of the condensation of dilute Bose gases [27]. From the physical point of view, such a frequency cutoff is not properly justified for classical waves. It turns out that an effective frequency cutoff arises naturally in the guided-wave configuration of the optical beam. The

frequency cutoff plays a key role in wave condensation since it prevents the divergence of the critical energy for condensation. Moreover, it has been shown that in two dimensions, wave condensation does not occur in the thermodynamic limit [24,26]. We show that a parabolic waveguide configuration reestablishes wave condensation in two dimensions, in analogy with quantum Bose-Einstein condensation. Accordingly, wave condensation and thermalization can be studied accurately through the analysis of the two-dimensional spatial evolution of a guided optical beam. To motivate the experimental confirmation of our predictions, the numerical simulations have been performed in the framework of a realistic nonlinear optics experiment that can be realized with currently available technology.

II. NLS MODEL

The experiment we have in mind refers to the propagation of an incoherent (speckle) beam in a multimode optical waveguide. We briefly sketch the derivation of the NLS model equation governing the propagation of the optical field [28]. The optical wave propagates along the z axis of the waveguide, which we assume to be translationally invariant along z. The propagation of the field amplitude is known to be ruled by the Helmholtz equation

$$\partial_{zz}\phi + \nabla^2\phi + \tilde{n}^2(\boldsymbol{r})k_0^2\phi = 0, \tag{1}$$

where $\boldsymbol{r} = (x,y)$ denotes the position in the transverse plane and ∇^2 denotes the corresponding transverse Laplacian. The index of refraction is $\tilde{n}(\boldsymbol{r})$ and $k_0 = 2\pi/\lambda$ is the wave number, λ being the vacuum wavelength of the monochromatic source. We assume that the variations of the linear refractive index $n(\boldsymbol{r})$ are relatively small (i.e., the so-called weak-guidance approximation). The small nonlinear contribution n_2 to the refractive index can be introduced as follows, $\tilde{n}^2(\boldsymbol{r}) \simeq n^2(\boldsymbol{r}) + 2n_0n_2I(\boldsymbol{r})$, where $I = |\phi|^2$ is the intensity and n_0 is a refractive index of reference [see Fig. 1(a)]. Under the assumption of the paraxial approximation, Eq. (1) then recovers the NLS equation [28]

$$i\partial_z A + \frac{1}{2k_0n_0}\nabla^2 A + \frac{k_0}{2n_0}\left[n^2(\boldsymbol{r}) - n_0^2\right]A + k_0n_2|A|^2A = 0, \tag{2}$$

where $A(\boldsymbol{r},z) = \phi(\boldsymbol{r},z)\exp(ik_0n_0z)$. As schematically illustrated in Fig. 1(a), we suppose that the optical waveguide exhibits a truncated shape, with a revolution symmetry with respect to the z axis. With the change of variable $\psi(\boldsymbol{r},z) = A(\boldsymbol{r},z)\exp(-iV_0z)$, where $V_0 = k_0(n_1^2 - n_0^2)/(2n_0)$ is the potential depth and n_1 the core refractive index at $\mathbf{r} = 0$ [Fig. 1(a)], Eq. (2) can be written in the following conventional form:

$$i\partial_z\psi = -\alpha\nabla^2\psi + V(\mathbf{r})\psi + \gamma|\psi|^2\psi, \tag{3}$$

where $\alpha = 1/(2k_0n_0)$, $\gamma = k_0n_2$, and

$$V(\mathbf{r}) = k_0\left(\frac{n_1^2 - n^2(\mathbf{r})}{2n_0}\right), \tag{4}$$

is the waveguide potential depicted in Fig. 1(b). Note that the depth of the waveguide potential is usually small, $[n_1^2 - n^2(\mathbf{r})]/2n_0 \simeq n_1 - n(\mathbf{r})$, so that $V(\mathbf{r}) \simeq k_0[n_1 - n(\mathbf{r})]$. We recall that the NLS Eq. (3) conserves the power of the optical field

$$N = \int |\psi|^2\, d\boldsymbol{r}, \tag{5}$$

and the total energy (Hamiltonian) $H = E + U$, which has a linear contribution

$$E = \int \alpha|\nabla\psi|^2\, d\boldsymbol{r} + \int V(r)|\psi|^2\, d\boldsymbol{r}, \tag{6}$$

and a nonlinear Kerr contribution

$$U = \frac{\gamma}{2}\int |\psi|^4\, d\boldsymbol{r}. \tag{7}$$

.

III. NUMERICAL SIMULATIONS

A. Experimental optical setting

Although this work is general and can be applied to different types of waveguide geometries characterized by different index profiles, we shall present below the numerical simulations within the concrete example of the parabolic index profile. Besides its natural importance for Bose-Einstein condensates [29], the parabolic potential is known to find a direct application in the propagation of an optical beam in a graded-index multimode optical fiber [28]. In the following we shall thus consider this optical setting in detail. In particular, we shall consider a parabolic index profile, as schematically depicted in Fig. 1(a). The corresponding potential reads $V(\mathbf{r}) = V_0(\frac{r}{a})^2$ for $|\mathbf{r}| \leqslant a$, $V(\mathbf{r}) = V_0$ for $|\mathbf{r}| > a$, where a is the fiber radius. We shall note $V(\mathbf{r}) = qr^2$, with $q = V_0/a^2$. Also, we shall assume that the number of modes of the multimode optical fiber is rather large, $M \simeq V_0^2/(2\beta_0^2) \gg 1$, where $\beta_0 = 2\sqrt{\alpha q}$ is the eigenvalue associated to the fundamental Gaussian mode.

The experimental configuration is conceptually simple. A (quasi)monochromatic beam is passed through a random phase mask to produce spatial random fluctuations. The beam is subsequently injected into the graded-index multimode optical fiber and we are interested in the evolution of the spatial coherence properties of the wave during its propagation. In the numerical simulations we considered realistic parameters that refer to typical multimode optical fibers available in the commerce. More precisely, we considered a fiber radius of $a = 15\ \mu$m and an index difference of $n_1 - n_0 = 6 \times 10^{-3}$,

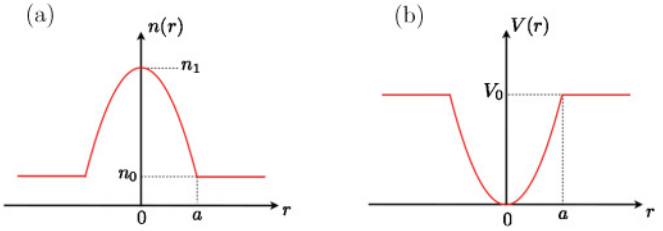

FIG. 1. (Color online) (a) Refractive index profile $n(r)$ of the optical waveguide and (b) corresponding confining potential $V(\mathbf{r})$ in the NLS Eq. (3).

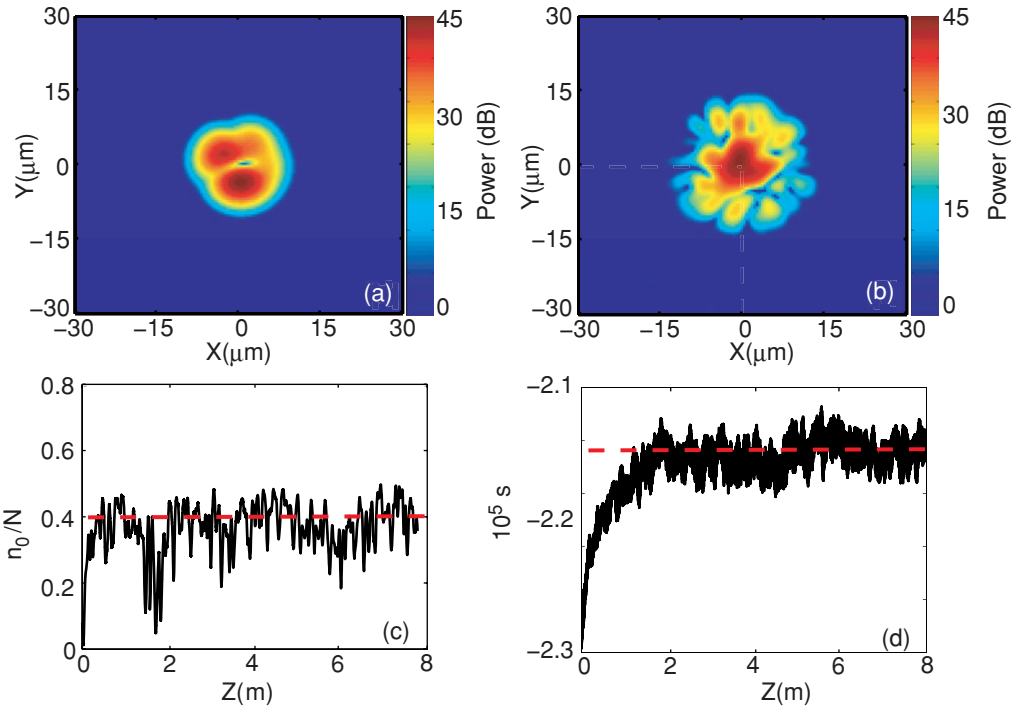

FIG. 2. (Color online) (a) Initial field intensity $|\psi|^2(\boldsymbol{r}, z = 0)$, and (b) corresponding intensity distribution at $z = 7$ m obtained by integrating numerically the NLS Eq. (3) (in 10Log_{10} scale). (c) Evolution of the fraction of condensed power n_0/N vs the propagation distance z. The horizontal dashed red line denotes the value of the condensate amplitude n_0^{eq}/N predicted by the theory [see Eqs. (23) and (24)]. (d) Corresponding evolution of the nonequilibrium entropy $\mathcal{S}$. Parameters of the simulation are given in the text.

with a refractive index of reference $n_0 = 1.45$. With these parameters the number of modes is $M = 66$.

It is important to note that silica fibers exhibit a focusing nonlinearity, $\gamma < 0$ in Eq. (3). The incoherent beam may thus exhibit filamentation effects (i.e., speckle beam fragmentation) during its propagation in the fiber. However, as revealed by the numerical simulations, the beam does not exhibit filamentation effects because we consider the weakly nonlinear regime of propagation, in which the linear energy dominates the nonlinear energy, $U/E \ll 1$. Note that this assumption will allow us to formulate a weak-turbulence theoretical description of the condensation process (see Sec. IV). This means that the nonlinearity plays a perturbative role when compared to linear effects resulting from the confining potential or from diffraction. The weakly nonlinear condition ($U/E \ll 1$) can easily be satisfied in the framework of the considered optical fiber system since the nonlinearity of silica fibers is known to be relatively small as compared to other types of commonly used nonlinear optical media. In the numerical simulations we considered the following standard value of the nonlinear silica coefficient $n_2 = -2 \times 10^{-8}\,\mu\text{m}^2/\text{W}$, together with a power of the beam of $N = 94$ kW. With these parameters we verified that, regardless of the initial degree of coherence of the wave injected into the fiber, the weakly nonlinear regime is still satisfied (i.e., the condition $U/E \ll 1$ is verified for all numerical points reported in the condensation curve in Fig. 4).

Note that the relatively high value of the power N of the beam is experimentally accessible by using laser sources delivering long pulses at a low-repetition rate. For instance, if one considers (quasimonochromatic) optical pulses in the nanosecond range, the power of the beam can be increased significantly, while temporal dispersion effects can be ignored. Indeed, the influence of group-velocity dispersion is known to be negligible with nanosecond optical pulses [28]. On the other hand, different optical modes travel with different group velocities into the fiber, thus leading to an effective temporal broadening of the pulse, a process known as "modal dispersion" [30]. With the parameters of the multimode fiber given above, the maximum temporal broadening due to modal dispersion is typically in the piscosecond range (∼0.9 ps) for a fiber length of about 15 meters. Considering that fiber lengths of $L \simeq 7$ m should be sufficient to get wave condensation (see the numerical simulation reported in Fig. 2), modal dispersion effects are negligible in the nanosecond pulse regime. Note that the power N considered in the simulations can be decreased substantially by simply increasing the fiber length. Accordingly, temporal dispersion effects can be ignored in the experimental configuration discussed above, which thus validates *a posteriori* the purely spatial NLS model considered in Sec. II [Eq. (3)].

Finally, it is important to underline that in the weakly nonlinear regime considered here ($U/E \ll 1$), the eigenmodes of the nonlinear problem are well approximated by the corresponding Gauss-Hermite modes of the linearized NLS Eq. (3) relevant to the ideal parabolic potential ($V_0 \to \infty$). However, because of the truncation of the parabolic potential [see Fig. 1(b)], the higher-order modes exhibit some deviations from the Gauss-Hermite modes (see, e.g., Fig. 5 in the Appendix). For this reason, we have calculated numerically the *exact eigenmodes and eigenvalues of the truncated potential*.

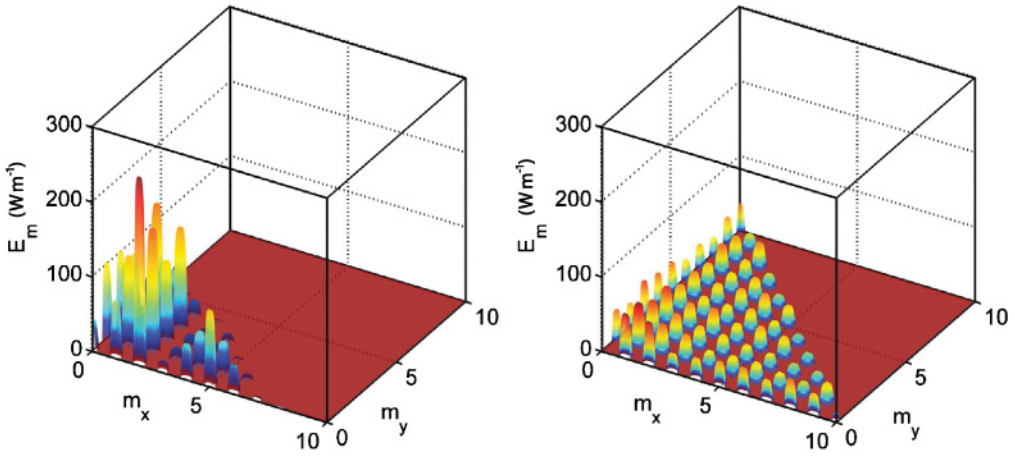

FIG. 3. (Color online) Numerical simulation of the NLS Eq. (3) showing the establishment of energy equipartition among the modes of the waveguide: Energy per mode $\mathcal{E}_m = \beta_m n_m$ [see Eq. (13)] vs the mode $m = (m_x, m_y)$, in (a) the initial condition and (b) averaged over the propagation once the equilibrium state is reached, i.e., $\partial_z \mathcal{S} \simeq 0$. The amount of power n_m in the mode $m = (m_x, m_y)$ is calculated by projecting the field amplitude into the corresponding eigenmode [see Eq. (12)]. Energy almost reaches an equipartition among all modes except the fundamental condensed mode $m_x = m_y = 0$ [not shown in (a–b)]. Parameters are the same as in Fig. 2 (see the text in Sec. III A). In particular, we considered a truncated parabolic potential (Fig. 1), so that $\beta_{m_x,m_y} \simeq \beta_0(m_x + m_y + 1)$ and only modes whose eigenvalue verifies $\beta_{m_x,m_y} \leqslant V_0$ are guided.

B. Numerical results

The numerical scheme used to integrate Eq. (3) is based on a standard beam propagation method. The accuracy of the numerical simulations increases significantly when the initial condition $\psi(\boldsymbol{r}, z = 0)$ is a random superposition of the modes of the truncated potential $V(\mathbf{r})$. Indeed, in this way the initial condition does not excite radiative modes that are not preserved during the propagation of the wave. We verified the accuracy of the simulations through the conservation of the Hamiltonian H and the total power N. The conservation of this latter quantity has also been checked by means of its modal expansion. Specifically, we verified the conservation of N by projecting the field amplitude $\psi(\boldsymbol{r}, z)$ on each guided mode of the *truncated potential* and then we added all modal contributions, as expressed by Eqs. (11) and (12) below. Along the same way, we verified that, during the propagation, the calculation of the linear energy E by means of its modal expansion (13) coincides with the corresponding integral expression given in Eq. (6).

A typical evolution of the intensity of the field $|\psi|^2(\boldsymbol{r}, z)$ is reported in Figs. 2(a) and 2(b). The initial condition is a random superposition of the modes of the truncated potential, as expressed by Eq. (8) below. The evolution of the field reported in Figs. 2(a) and 2(b) shows two main features of wave condensation. On the one hand, small-scale fluctuations carrying a negligible amount of power tend to populate higher-order modes. On the other hand, the power of the wave tends to concentrate into the center of the waveguide, so that the fundamental mode gets "macroscopically" populated. This condensation process is a consequence of the natural irreversible thermalization of the optical wave to equilibrium. This aspect was originally pointed out in the framework of extensive numerical simulations of the so-called "projected Gross-Pitaevskii equation," whose study was aimed at providing a classical description of thermal (i.e., finite temperature) Bose-Einstein condensed gases [27]. The condensation effect is illustrated in Fig. 2(c), which reports the evolution of the fraction of power condensed into the fundamental mode n_0/N as a function of the propagation distance z. The amount of condensed power is calculated by projecting the field amplitude ψ into the fundamental mode [see below Eq. (12) for details]. As illustrated in Fig. 2(c), n_0/N increases and slowly saturates as the optical field reaches the equilibrium state. This irreversible process of thermalization is corroborated by the saturation of the production of (nonequilibrium) entropy reported in Fig. 2(d), a peculiar property described by the H theorem of entropy growth (see Sec. IV B). The main feature that characterizes this thermalization of the wave becomes apparent through the analysis of the distribution of the energy among the modes of the waveguide. As remarkably illustrated in Fig. 3, the optical field relaxes toward an equilibrium state in which the energy is equipartitioned among all the modes on average, except for the fundamental condensed mode which is macroscopically populated (not shown in Fig. 3). In this figure, the energy per mode $\mathcal{E}_m$ [$m = (m_x, m_y)$] has been calculated by projecting the field amplitude on all the modes of the truncated potential [see Eqs. (12) and (11)], and then an average over the propagation distance has been taken once the equilibrium state was reached.

To summarize, the condensation process is characterized by an irreversible transfer of the power of the field toward the fundamental mode ("condensate"). Note that all the power of the initial incoherent wave cannot be completely transferred to the fundamental mode because such evolution would imply a loss of information for the field, which would violate the *formal* reversibility of the system. Actually, the fundamental mode remains immersed in a sea of small-scale fluctuations (uncondensed "quasiparticles"), whose energy is equipartitioned among all the modes of the waveguide. These thermalized small-scale fluctuations store the information necessary for a reversible evolution of the wave, consistent with the formal reversibility of the NLS Eq. (3). The theoretical

analysis of this condensation process is the subject of the next section.

IV. WAVE TURBULENCE APPROACH

To describe this condensation process analytically, we formulate a WT description of the random field into the basis of the eigenmodes of the potential $V(\mathbf{r})$. This approach differs from the conventional WT approach [20–22] in which the random wave exhibits a homogeneous statistics [$V(\mathbf{r}) = 0$ in Eq. (3)], so that the wave amplitude is expanded into the usual Fourier (plane-wave) basis with periodic boundary conditions (see the Appendix, Sec. 2) [31]. Note that, although we considered the concrete example of the parabolic index profile in the simulations, the theoretical approach we are going to present can be applied to different types of potentials $V(\mathbf{r})$.

A. Basic considerations

We assume that the initial random field $\psi(z = 0,\boldsymbol{r})$ can be expanded into the orthonormal basis of the eigenmodes of the linearized NLS equation [Eq. (3) with $\gamma = 0$]

$$\psi(\boldsymbol{r},z = 0) = \sum_m c_m(z = 0)\, u_m(\boldsymbol{r}), \tag{8}$$

where the index $\{m\}$ labels the two numbers (m_x,m_y) needed to specify the mode that $u_m(\boldsymbol{r})$ refers to. The modal coefficients are random variables uncorrelated with one another, $\langle c_m(z = 0)c_n^*(z = 0)\rangle = n_m(z = 0)\,\delta^K_{n,m}$, $\delta^K_{n,m}$ being the Kronecker's symbol. We remark that this formalism is also known as the Karhunen-Loeve expansion [32]. The eigenmodes $u_m(\boldsymbol{r})$ are orthonormal, $\int u_m(\mathbf{r})\,u_n^*(\boldsymbol{r})\,d\boldsymbol{r} = \delta^K_{n,m}$, and satisfy the "stationary" (i.e., z independent) Schrödinger equation

$$\beta_m u_m(\boldsymbol{r}) = -\alpha\nabla^2 u_m(\boldsymbol{r}) + V(\boldsymbol{r})u_m(\boldsymbol{r}), \tag{9}$$

with the corresponding eigenvalues β_m. In the ideal parabolic potential ($V_0 \to \infty$), $u_m(\boldsymbol{r})$ refer to the normalized Hermite-Gaussian functions with corresponding eigenvalues $\beta_m = \beta_{m_x,m_y} = \beta_0(m_x + m_y + 1)$, $u_{m_x,m_y}(x,y) = \kappa(\pi m_x!\, m_y!\, 2^{m_x+m_y})^{-1/2}\, H_{m_x}(\kappa x)\, H_{m_y}(\kappa y)\, \exp[-\kappa^2(x^2+y^2)/2]$, where $\kappa = (q/\alpha)^{1/4}$.

As it propagates through the waveguide the incoherent field $\psi(z,\boldsymbol{r})$ can be represented as a superposition of modal waves with random coefficients $c_m(z)$, which denotes the respective modal occupancy

$$\psi(\boldsymbol{r},z) = \sum_m c_m(z)\, u_m(\boldsymbol{r})\, \exp(-i\beta_m z). \tag{10}$$

In the linear regime of propagation $\gamma = 0$, we have $c_m(z) = c_m(z = 0)$. In the nonlinear regime, we shall follow in the next section the procedure of the random phase approximation underlying the WT theory [20–22]. In particular, the modal occupancies $c_m(z)$ are still random variables uncorrelated with one another, $\langle c_m(z)c_n^*(z)\rangle = n_m(z)\,\delta^K_{n,m}$. The modal occupancies $n_m(z)$ satisfy a coupled system of nonlinear equations that we shall describe in Sec. IV B.

The average local power of the field is $\langle|\psi(\boldsymbol{r},z)|^2\rangle = \sum_m n_m(z)\,|u_m(\boldsymbol{r})|^2$, which depends on the spatial variable $\boldsymbol{r}$ because the statistics of the field is not homogeneous. A spatial integration over $\boldsymbol{r}$ gives the total average power of the beam

$$N = \sum_m n_m(z), \tag{11}$$

which is a conserved quantity. The parameter $n_m(z)$ thus denotes the amount of power in the mode $\{m\}$. It can be obtained by projecting the field $\psi(z,\boldsymbol{r})$ on the corresponding eigenmode $u_m(\boldsymbol{r})$

$$n_m(z) = \left\langle \left| \int \psi(\boldsymbol{r},z)\, u_m^*(\boldsymbol{r})\, d\boldsymbol{r} \right|^2 \right\rangle = \langle |c_m(z)|^2\rangle. \tag{12}$$

Wave condensation takes place when the fundamental mode becomes macroscopically populated (i.e., when $n_0 \gg n_m$ for $m \neq 0$) [29,33].

In the same way, by substituting the modal expansion of the incoherent field $\psi(z,\boldsymbol{r})$ into the expression of the linear energy (6), one obtains

$$E(z) = \sum_m \mathcal{E}_m(z) = \sum_m n_m(z)\,\beta_m. \tag{13}$$

The total linear energy is the sum of the modal energies weighted by the corresponding modal occupancy $n_m(z)$.

B. Kinetic equation

We now study the influence of a weak nonlinear coupling among the modes, so that the modal occupancies defined by Eq. (12) depend on z, $n_m(z)$. This weakly nonlinear regime precisely corresponds to the regime investigated numerically in Sec. III B. Substituting the modal expansion (10) into the NLS Eq. (3), one obtains

$$i\,\partial_z a_m = \beta_m a_m + \gamma \sum_{p,q,s} W_{mpqs} a_p a_q^* a_s, \tag{14}$$

where $a_m(z) = c_m(z)\, \exp(-i\beta_m z)$, and the fourth-order tensor is defined by the overlap integral

$$W_{mpqs} = \int u_m^*(\boldsymbol{r}) u_p(\boldsymbol{r}) u_q^*(\boldsymbol{r}) u_s(\boldsymbol{r})\, d\boldsymbol{r}. \tag{15}$$

Equation (14) conserves the total power $N = \sum_m |a_m|^2$ and the Hamiltonian

$$H = \sum_m \beta_m |a_m|^2 + \frac{\gamma}{4} \sum_{m,p,q,s} (W_{mpqs} a_m^* a_p a_q^* a_s + W_{mpqs}^* a_m a_p^* a_q a_s^*). \tag{16}$$

Starting from Eq. (14) and following the procedure of the random phase approximation [21,22], we derive in the Appendix an irreversible kinetic equation governing the nonlinear evolution of the modal occupancies. For this purpose, we take the continuum limit of the discrete sum over the modes $\{m\}$, which is justified when one deals with a large number of modes (i.e., $V_0/\beta_0 \gg 1$). The substitution of the discrete sums by continuous integrals corresponds to the so-called "semiclassical description of the excited states" [29]. Its validity implies that the relevant excitation energies contributing to the discrete sum are much larger than the level spacing β_0 (i.e., the spreading of the modal occupancies is much larger than β_0). In the Appendix we derive the following

kinetic equation governing the irreversible evolution of the modal occupancies

$$\partial_z \tilde{n}_{\boldsymbol{\kappa}}(z) = \frac{4\pi\gamma^2}{\beta_0^6} \iiint d\boldsymbol{\kappa}_1 d\boldsymbol{\kappa}_2 d\boldsymbol{\kappa}_3 \delta\left(\tilde{\beta}_{\boldsymbol{\kappa}_1} + \tilde{\beta}_{\boldsymbol{\kappa}_3} - \tilde{\beta}_{\boldsymbol{\kappa}_2} - \tilde{\beta}_{\boldsymbol{\kappa}}\right) \times \left|\tilde{W}_{\boldsymbol{\kappa}\boldsymbol{\kappa}_1\boldsymbol{\kappa}_2\boldsymbol{\kappa}_3}\right|^2 \tilde{n}_{\boldsymbol{\kappa}} \tilde{n}_{\boldsymbol{\kappa}_1} \tilde{n}_{\boldsymbol{\kappa}_2} \tilde{n}_{\boldsymbol{\kappa}_3} \left(\tilde{n}_{\boldsymbol{\kappa}}^{-1} + \tilde{n}_{\boldsymbol{\kappa}_2}^{-1} - \tilde{n}_{\boldsymbol{\kappa}_1}^{-1} - \tilde{n}_{\boldsymbol{\kappa}_3}^{-1}\right) + \frac{8\pi\gamma^2}{\beta_0^2} \int d\boldsymbol{\kappa}_1 \delta\left(\tilde{\beta}_{\boldsymbol{\kappa}_1} - \tilde{\beta}_{\boldsymbol{\kappa}}\right) \left|\tilde{U}_{\boldsymbol{\kappa}\boldsymbol{\kappa}_1}(\tilde{\mathbf{n}})\right|^2 \left(\tilde{n}_{\boldsymbol{\kappa}_1} - \tilde{n}_{\boldsymbol{\kappa}}\right), \tag{17}$$

where

$$\tilde{U}_{\boldsymbol{\kappa}\boldsymbol{\kappa}_1}(\tilde{\mathbf{n}}) = \frac{1}{\beta_0^2} \int d\boldsymbol{\kappa}' \, \tilde{W}_{\boldsymbol{\kappa}\boldsymbol{\kappa}_1\boldsymbol{\kappa}'\boldsymbol{\kappa}'} \, \tilde{n}_{\boldsymbol{\kappa}'}. \tag{18}$$

The functions with a tilde refer to the natural continuum extension of the corresponding discrete functions, that is, $\tilde{n}_{\boldsymbol{k}}(z) = n_{[\boldsymbol{k}/\beta_0]}(z)$, $\tilde{\beta}_{\boldsymbol{\kappa}} = \beta_{[\boldsymbol{\kappa}/\beta_0]}$, $\tilde{W}_{\boldsymbol{\kappa}\boldsymbol{\kappa}_1\boldsymbol{\kappa}_2\boldsymbol{\kappa}_3} = W_{[\boldsymbol{\kappa}/\beta_0][\boldsymbol{\kappa}_1/\beta_0][\boldsymbol{\kappa}_2/\beta_0][\boldsymbol{\kappa}_3/\beta_0]}$ and so on, where $[x]$ denotes the integer part of x. The kinetic Eqs. (17) and (18) are general and, in principle, relevant to different types of waveguide configurations (see the Appendix, Sec. 3). In the particular case of the ideal parabolic potential of infinite depth, we have $\tilde{\beta}_{\boldsymbol{\kappa}} = \kappa_x + \kappa_y + \beta_0$. This expression plays the role of a generalized *anisotropic* dispersion relation whose wave vector reads $\boldsymbol{\kappa} = \beta_0(m_x, m_y)$.

The kinetic Eqs. (17) and (18) differs from the conventional wave turbulence kinetic equation in some various respects. First, we remark the presence of the new second term in Eq. (17). Note that this term vanishes when the occupation of a mode depends only on its energy $\tilde{\beta}$. Actually, this term enforces an isotropization of the mode occupancies among the modes with the same modal energy. Another important property of the kinetic Eq. (17) is the presence of the function $\tilde{W}_{\boldsymbol{\kappa}\boldsymbol{\kappa}_1\boldsymbol{\kappa}_2\boldsymbol{\kappa}_3}$ in the collision term. To comment on this function, let us consider the homogeneous problem [$V(\mathbf{r}) = 0$ in Eq. (3)], where the field amplitude (10) is usually expanded in the plane-wave basis $u_{m_x,m_y}(\boldsymbol{r}) = \frac{1}{L}\exp[2i\pi(m_x x + m_y y)/L]$, L being the box size. In this case the function $|W_{\boldsymbol{\kappa}\boldsymbol{\kappa}_1\boldsymbol{\kappa}_2\boldsymbol{\kappa}_3}|^2$ recovers the familiar Dirac δ function (see the Appendix, Sec. 2), which guarantees momentum conservation at each elementary collision of two quasiparticles. This is consistent with the fact that the presence of the inhomogeneous potential $V(r)$ in Eq. (3) breaks the conservation of the momentum. Also note that, in the particular case of the Fourier plane-wave expansion, the second term in the kinetic Eq. (17) vanishes identically, so that it recovers the conventional WT kinetic equation (see the Appendix, Sec. 2).

The kinetic Eqs. (17) adn (18) conserve the power $N = \beta_0^{-2}\int d\boldsymbol{\kappa}\tilde{n}_{\boldsymbol{\kappa}}$ and the energy $E = \beta_0^{-2}\int d\boldsymbol{\kappa}\tilde{\beta}_{\boldsymbol{\kappa}}\tilde{n}_{\boldsymbol{\kappa}}$. The *irreversible* property of the kinetic equation (17) is expressed by a H theorem of entropy growth $d\mathcal{S}/dz \geqslant 0$, where the nonequilibrium entropy reads $\mathcal{S}(z) = \beta_0^{-2}\int d\boldsymbol{\kappa}\ln(\tilde{n}_{\boldsymbol{\kappa}})$. Actually, the first term of Eq. (17) enforces the mode occupancies to reach the "most disordered" stationary distribution. The Rayleigh-Jeans equilibrium state $\tilde{n}_{\boldsymbol{\kappa}}^{\mathrm{eq}}$ realizing the maximum of entropy, subject to the constraints of conservation of E and N, is obtained by introducing the corresponding Lagrange's multipliers

$$\tilde{n}_{\boldsymbol{\kappa}}^{\mathrm{eq}} = \frac{T}{\tilde{\beta}_{\boldsymbol{\kappa}} - \mu}, \tag{19}$$

where, by analogy with thermodynamics, T denotes the temperature and μ the chemical potential. In particular, the temperature denotes the amount of energy $\tilde{\mathcal{E}}_{\boldsymbol{\kappa}}$ that is equipartitioned among the modes of the waveguide. Indeed, in the tails of the equilibrium distribution (19) (i.e., $\tilde{\beta}_{\boldsymbol{\kappa}} \gg |\mu|$) we have $\tilde{\mathcal{E}}_{\boldsymbol{\kappa}} = \tilde{\beta}_{\boldsymbol{\kappa}}\,\tilde{n}_{\boldsymbol{\kappa}}^{\mathrm{eq}} \sim T$ [see Eq. (13)]. This equilibrium property of energy equipartition was confirmed by the numerical simulations in Fig. 3. Also note that the equilibrium state (19) cancels both collision terms of the kinetic Eqs. (17) and (18). Finally, we remark that the equilibrium distribution (19) exhibits a divergence for $\mu = \beta_0$. This property entails condensation into the fundamental (Gaussian) mode of the waveguide irrespective of the sign of the nonlinearity, which may be either focusing or defocusing. This is consistent with the fact that the kinetic Eq. (17) is not sensitive to the sign of the nonlinearity (i.e., it only depends on γ^2). Note that this contrasts with the usual condensation process in the homogeneous problem [$V(\mathbf{r}) = 0$]: depending on the sign of the nonlinearity, wave condensation manifests itself either by the generation of a soliton (focusing regime) [34] or a plane wave (defocusing regime) [23,24]. Below we shall analyze the process of condensation in a waveguide in more detail.

C. Frequency cutoff, density of states, and thermodynamic limit

The number of modes involved in the dynamics is finite because of the truncation of the potential ($V_0 < \infty$). In this way the truncated potential introduces an effective frequency cutoff for the classical nonlinear wave because modes whose eigenvalues exceed the potential depth $\tilde{\beta}_{\boldsymbol{\kappa}} > V_0$ are not guided during the propagation. A more rigorous justification of this aspect is given in the Appendix, Sec. 4. Note that this is in contrast with the homogeneous problem [$V(\mathbf{r}) = 0$ in Eq. (3)] where the wave amplitude ψ is expanded into the plane-wave basis. In this case, the frequency cutoff k_c is introduced in an artificial way through the spatial discretization (dx) of the NLS equation (i.e., $k_c = \pi/dx$) so that in the continuous limit $k_c \to \infty$ (see, e.g., Ref. [24]).

Let us discuss the importance of the truncation of the potential ($V_0 < \infty$) through the example of the parabolic potential considered in the numerical simulations in Sec. III B. Considering the constraint $\beta_0 \leqslant \tilde{\beta}(\boldsymbol{\kappa}) \leqslant V_0$, as well as the assumption $\beta_0 \ll V_0$ (i.e., $M \gg 1$), the power of the field at equilibrium reads $N = (T/\beta_0^2)\int_0^{V_0} d\kappa_x \int_0^{V_0-\kappa_x} (\kappa_x + \kappa_y + \beta_0 - \mu)^{-1} d\kappa_y$, which gives

$$N = \frac{T}{\beta_0^2}\left[V_0 - \tilde{\mu}\ln\left(\frac{-\tilde{\mu}}{V_0 - \tilde{\mu}}\right)\right], \tag{20}$$

where we defined $\tilde{\mu} = \mu - \beta_0$. To comment on expression (20), we recall that in the homogeneous problem [$V(\mathbf{r}) = 0$ in Eq. (3)] wave condensation was shown to only occur in three dimensions (3D), while in two dimensions (2D) the chemical potential was shown to reach zero for a vanishing temperature [8,24,26]. In analogy with Bose-Einstein condensation in quantum gases, this means that wave condensation does not occur in the thermodynamic limit in 2D. Conversely, Eq. (20) reveals that $\tilde{\mu} \to 0$ for a nonvanishing critical temperature, $T_c = 4\alpha N q/V_0$, which indicates that the presence of a parabolic potential $V(\mathbf{r})$ reestablishes wave condensation in the thermodynamic limit in 2D. Indeed, the thermodynamic

limit for a parabolic potential corresponds to taking $N \to \infty$ and $q \to 0$, keeping constant the product Nq [29]. This result is in complete analogy with the well-known fact that a parabolic potential reestablishes Bose-Einstein condensation in 2D [29]. There is, however, a difference with quantum condensation. Bose-Einstein condensation is known to be reestablished in a parabolic potential of infinite depth $V_0 \to \infty$, while here T_c tends to zero in the limit $V_0 \to \infty$. Contrary to the quantum case, one also needs to introduce a finite depth of the potential $V_0 < \infty$ to get wave condensation in 2D. This condition is obviously satisfied for any optical waveguide configuration.

Note that the same conclusion is reached through the analysis of the density of states, $\rho(\beta) = \frac{1}{\beta_0^2} \iint_{\mathcal{D}} d^2\boldsymbol{\kappa}\, \delta(\beta - \kappa_x - \kappa_x - \beta_0)$, where the domain of integration $\mathcal{D}$ denotes $\iint_{\mathcal{D}} d^2\boldsymbol{\kappa} = \int_0^{V_0} d\kappa_x \int_0^{V_0-\kappa_x} d\kappa_y$. As for quantum Bose gases, the presence of a parabolic potential leads to $\rho(\beta) \propto \beta$. Specifically, in the limit $\beta_0/V_0 \ll 1$, we have $\rho(\beta) = \beta/\beta_0^2$ for $\beta \leqslant V_0$, and $\rho(\beta) = 0$ for $\beta > V_0$. Note that the number of modes simply reads $M \simeq \int_0^{V_0} \rho(\beta)\, d\beta = V_0^2/(2\beta_0^2)$. According to this expression of $\rho(\beta)$ and considering the limit $\tilde{\mu} \to 0$, the infrared convergence of the integral $N = \int_0^{V_0} d\beta\, \rho(\beta)\, n_\beta^{\mathrm{eq}} = T \int_0^{V_0} d\beta\, \rho(\beta)/\beta$ is ensured by the linear dependence of the density of states $\rho(\beta) \propto \beta$. However, the ultraviolet convergence of N requires $V_0 < \infty$, while it is ensured by the exponential term of the Bose distribution in the quantum case.

D. Condensate fraction

We shall now look for a relation between the fraction of condensed power n_0/N and the temperature T or the energy E. Note that, to avoid cumbersome notations, in the following we shall denote by n_0 the condensate amplitude that the field has reached at equilibrium (i.e., $n_0^{\mathrm{eq}} \equiv n_0$). As in the usual interpretation of Bose-Einstein condensation, we set $\mu = \beta_0$ in the equilibrium distribution (19). Note that the assumption $\tilde{\mu} = \mu - \beta_0 = 0$ for $T \leqslant T_c$ can be justified rigorously in the 2D thermodynamic limit. Isolating the fundamental mode, one has $N - n_0 = (T/\beta_0^2) \iint_{\mathcal{D}} 1/(\kappa_x + \kappa_y)\, d^2\boldsymbol{\kappa}$, where $n_0 = T/[\beta_0^2(\beta_0 - \mu)]$. We thus readily obtain $N - n_0 = TV_0/\beta_0^2$. Proceeding in a similar way for the energy, one obtains $E - n_0\beta_0 = \frac{TV_0^2}{2\beta_0^2}(1 + 2\beta_0/V_0)$. Eliminating the temperature from the expressions for E and N gives the following expression of the condensate fraction

$$\frac{n_0}{N} = 1 - \frac{E - E_0}{NV_0/2}, \tag{21}$$

where $E_0 = N\beta_0$ refers to the minimum energy (i.e., the energy of the field when all the power is condensed, $n_0/N = 1$). The condensate amplitude n_0/N increases as the energy E decreases, and condensation arises below the critical energy

$$E_c = E_0 + NV_0/2 = \frac{NV_0}{2}\left(1 + \frac{2\beta_0}{V_0}\right). \tag{22}$$

This expression deserves to be commented on in two respects. First, because of the truncation of the waveguide potential ($V_0 < \infty$), the value of E_c does not diverge to infinity. This is in contrast with the homogeneous problem [$V(r) = 0$ in Eq. (3)] and the plane-wave expansion (see the Appendix). In this case the critical value of the energy behaves as $E_c^{\mathrm{hom}} \sim Nk_c^2/\ln(k_c)$, where $k_c = \pi/dx$ is the arbitrary frequency cutoff. In the continuous limit in which the spatial discretization of the NLS equation tends to zero, $dx \to 0$, the critical value of the energy E_c^{hom} diverges to infinity (see, e.g., Refs. [24,26]). A second point that could be remarked in Eq. (22) is that wave condensation is reestablished in the thermodynamic limit in 2D. Indeed, writing Eq. (22) in the following form, $E_c/S = Nq(1 + 2\beta_0/V_0)/(2\pi)$, where $S = \pi a^2$ is the waveguide surface, it becomes apparent that the energy density E_c/S does not tend to zero in the thermodynamic limit ($N \to \infty, q \to 0$, keeping Nq constant). As discussed in Sec. IV C, this is again in contrast with the homogeneous problem and the plane-wave expansion of the field, in which E_c^{hom}/S tends to zero logarithmically in the thermodynamic limit [8,26].

The simple analysis of Eqs. (21) and (22) outlined above provides physical insight into the process of wave condensation. However, a direct quantitative comparison with the numerical simulations requires an improved treatment. For this purpose, we shall follow the procedures outlined in Refs. [24,26] to improve Eq. (21). In the previous works [24,26] wave condensation was considered in the absence of a confining potential [$V(\mathbf{r}) = 0$ in Eq. (3)]. We generalize here these approaches by considering the modal expansion (10) into the eigenmodes of the potential $V(\mathbf{r})$.

Equation (21) can be improved along three lines. (i) It proves convenient to replace the continuous integrals by a discrete sum over the modes of the waveguide, a feature that was discussed in detail in Ref. [24]. Proceeding in a way similar as above, one obtains $n_0/N = 1 - (E - E_0)\sum'(m_x + m_y)^{-1}/[E_0(M - 1)]$, where M is the number of modes of the waveguide, and $\sum'$ denotes the sum over all modes $\{m = (m_x, m_y)\}$ excluding the fundamental mode $m = 0$. In the continuous limit we have $\sum' \frac{1}{m_x + m_y} \to \beta_0^{-1} \iint_{\mathcal{D}} \frac{d^2\boldsymbol{\kappa}}{\kappa_x + \kappa_y} = V_0/\beta_0$ and the number of modes $M = \beta_0^{-2} \iint_{\mathcal{D}} d^2\boldsymbol{\kappa} = V_0^2/(2\beta_0^2)$, so that the above equation recovers Eq. (21). (ii) A generalization of the expression of the condensate fraction, n_0/N versus E, can be done beyond the thermodynamic limit [8,26] (i.e., without the implicit assumption $\tilde{\mu} = 0$ for $T \leqslant T_c$). From the physical point of view, this means that we take into account the finite size of the optical waveguide. (iii) We include the contribution of the nonlinear energy U into the expression of the condensation curve. For this purpose, we split the contribution of the fundamental mode into the modal expansion of the field $\psi(z,\boldsymbol{r}) = \psi_0(z,\boldsymbol{r}) + \varepsilon(z,\boldsymbol{r})$, where $\psi_0(z,\boldsymbol{r}) = c_0(z)u_0(r)\exp(-i\beta_0 z)$ is the coherent condensate contribution and $\varepsilon(z,\boldsymbol{r}) = \sum_{m\neq 0} c_m(z)u_m(\boldsymbol{r})\exp(-i\beta_m z)$ is the incoherent contribution. This expansion can be substituted into the expression of U in Eq. (7), and making use of the random phase approximation, we obtain $\langle U\rangle = \gamma(\frac{1}{2}n_0^2\rho + 2n_0\sum_{j\neq 0} n_j W_{00jj} + \sum_{j\neq 0,k\neq 0} n_j n_k W_{jjkk})$, where $\rho = \int u_0^4(r)d\boldsymbol{r} = \kappa^2/(2\pi)$. At equilibrium, n_j and n_k in the above sum can be substituted by the corresponding equilibrium distributions.

The generalizations (i), (ii), and (iii) finally lead to the following expression of the condensation curve beyond the

thermodynamic limit, including the nonlinear contribution of the energy

$$\frac{n_0}{N}(\tilde{\mu}) = \frac{1}{-\tilde{\mu}\sum_m \frac{1}{\beta_m-\beta_0-\tilde{\mu}}}, \tag{23}$$

$$\langle H\rangle(\tilde{\mu}) = N\frac{\sum_m \frac{\beta_m}{\beta_m-\beta_0-\tilde{\mu}}}{\sum_m \frac{1}{\beta_m-\beta_0-\tilde{\mu}}} + \langle U\rangle(\tilde{\mu}), \tag{24}$$

where

$$\langle U\rangle(\tilde{\mu}) = \gamma\left[\frac{\rho}{2}n_0^2 - 2n_0^2\tilde{\mu}\int |u_0|^2(\mathbf{r})\sum_m{}' \frac{|u_m(\boldsymbol{r})|^2}{\beta_m-\beta_0-\tilde{\mu}}\,d\boldsymbol{r} + n_0^2\tilde{\mu}^2\int\left(\sum_m{}' \frac{|u_m(\boldsymbol{r})|^2}{\beta_m-\beta_0-\tilde{\mu}}\right)^2 d\boldsymbol{r}\right]. \tag{25}$$

The fraction of condensed power n_0/N is thus coupled to the total energy $\langle H\rangle$ through the nonvanishing chemical potential $\tilde{\mu} = \mu - \beta_0 \neq 0$. The parametric plot of Eqs. (23) and (24) with respect to $\tilde{\mu}$ is reported in Fig. 4 (continuous line). It is important to note the long tail in the condensation curve at high energies H, which is due to the nonvanishing chemical potential $\tilde{\mu} \neq 0$. In the thermodynamic limit $\tilde{\mu} \to 0$, the condensation curve (23) and (24) recovers the straight line discussed above through Eqs. (21) and (22) (see the dashed line in Fig. 4). Let us remark the good agreement between the theoretical condensation curve and the simulations, without using adjustable parameters. Note, however, that, due to the very long times required to reach equilibrium, this good agreement has not been confirmed with waveguides characterized by a larger number of modes. Indeed, the simulations reveal that the thermalization process slows down significantly as the number of modes of the waveguide is increased. A qualitative analysis of the kinetic Eq. (17) indicates that the long transients required to achieve wave thermalization are due to the intricate properties of the function $\tilde{W}_{\kappa_1\kappa_2\kappa_3\kappa_4}$ involved in the collision term.

We also note that the expression of $\langle U\rangle$ in Eq. (25) is rather involved. This is due to the nontrivial modal expansion (10) of the field ψ, which prevents the factorization of the integration over $\boldsymbol{r}$ with respect to the sum over the modes $\{m\}$. In the usual homogeneous problem [$V(\mathbf{r}) = 0$] and the plane-wave expansion, Eq. (25) recovers the following simplified expression obtained in Ref. [26], namely $\langle U\rangle = \gamma(n^2 - \frac{1}{2}n_0^2)$, where n and n_0 refer here to the densities of the power and of the condensate, respectively.

We finally underline that Eqs. (23) and (24) are valid for various different types of waveguide index profiles, provided one makes use of the appropriate eigenvalues β_m and eigenmodes $u_m(\boldsymbol{r})$. We note in this respect that we used the eigenvalues and eigenmodes of the *truncated* parabolic potential to plot Eqs. (23) and (24) in Fig. 4. The values of β_m and $u_m(\boldsymbol{r})$ for the truncated potential have been calculated numerically and they have been found to be well approximated by the corresponding analytical expressions given by the Gauss-Hermite expansion ($V_0 \to \infty$).

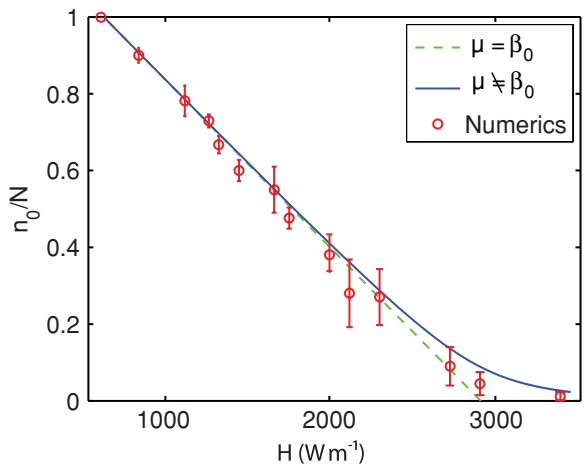

FIG. 4. (Color online) Fraction of power condensed in the fundamental mode at equilibrium n_0/N vs the energy of the field H for a truncated parabolic potential (parameters are given in Sec. III A). The red points refer to the results of the numerical simulations. They have been obtained by averaging n_0/N over the propagation distance once the equilibrium state is reached, i.e., $\partial_z\mathcal{S} \simeq 0$. The "error-bars" denote the amount of fluctuations (standard deviation) of n_0/N once equilibrium is reached. The continuous blue line refers to the theoretical condensation curve given in Eqs. (23)–(25), while the dashed green line refers to the corresponding thermodynamic limit [$\tilde{\mu} \to 0$ in Eqs. (23)–(25)]. In these plots the eigenvalues β_m and eigenmodes $u_m(\boldsymbol{r})$ in Eqs.(23)–(25) account for the truncation of the potential ($V_0 < \infty$). Note that the units of the Hamiltonian H are determined from its definition [see Eqs. (6) and (7)].

V. CONCLUSION AND PERSPECTIVES

In summary, we studied the thermalization and the condensation of a random nonlinear wave that propagates in an optical waveguide. The guided configuration provides a physical meaning to the frequency cutoff, which is usually introduced in an arbitrary way in the conventional description of wave condensation in the homogeneous problem. We formulated a wave turbulence description of the random nonlinear wave into the basis of the eigenmodes of the waveguide. As a result of the inhomogeneous statistics of the spatially confined random field, the kinetic Eq. (17) exhibits a novel term, which enforces an isotropization of the mode occupancies among the modes with the same energy. The analysis of the equilibrium distribution reveals that a parabolic potential reestablishes wave condensation in the thermodynamic limit in 2D. This is in analogy with quantum Bose-Einstein condensation. However, for classical wave condensation the parabolic potential also needs to be truncated, so as to ensure the ultraviolet convergence of N, and to prevent the divergence of the critical energy for condensation E_c. A closed relation between the condensate amplitude n_0 and the energy of the wave H has been derived, and has been found in quantitative agreement with the numerical simulations without adjustable parameters. The simulations have been performed in a realistic experimental configuration in which a speckle beam is injected in a graded index multimode optical fiber. In particular, they confirm the emergence of an energy equipartition among the modes of the waveguide, as described by the theoretical equilibrium distribution. Note that the thermal nonlinearity of silica fibers may also be exploited to enhance the nonlinear coefficient

[35]. Besides the optical fiber system, the experimental study of wave condensation can be envisaged in other types of waveguides (e.g., by exploiting the high nonlinearity of liquid crystals or photorefractives).

We finally briefly comment on some natural possible extensions of this work. For instance, the important problem of understanding the effect of disorder in nonlinear wave systems is the subject of current intense investigations, in particular, in the context of Bose-Einstein condensates [36]. The WT theory can provide some new physical insights into this vast problem. In particular, the thermalization of the nonlinear wave in a random potential $V(\boldsymbol{r})$ is expected to be highly affected by the spatially localized nature of Anderson modes, a feature that can be described by the collision term of the kinetic Eq. (17). On the other hand, the WT theory is known to provide an accurate description of fully developed turbulence in the weakly nonlinear regime [22]. It would be interesting to study optical turbulence in the waveguide configuration, in the presence of sources and sinks so as to drive the system far from equilibrium. A starting point to consider this problem could be the study of the existence of stationary nonequilibrium distributions (i.e., Zakharov-Kolmogorov spectra) in the kinetic equation derived here. This approach can also be relevant to the analysis of the dynamics of random lasers [12,16]. Finally, another nontrivial extension of the present work could be the study of optical wave thermalization and condensation in a waveguide characterized by a "chaotic" multimode cross section [37]. Indeed, the vast issue of "wave chaos" has been only studied in the context of the linear propagation of the waves, while the nonlinear regime has not been considered so far. More precisely, chaotic waveguides are known to be characterized by the existence of peculiar modes, termed "scar modes" [38]. It would be interesting to study the role of these modes in the process of nonlinear wave thermalization discussed here. These aspects will be the subject of future investigations.

ACKNOWLEDGMENTS

This work was supported by the Agence Nationale de la Recherche (ANR COSTUME and MANUREVA Projects No. ANR-08-SYSC-004-03 and No. ANR-08-SYSC-019, respectively). The authors thank H. R. Jauslin, R. Kaiser, and S. Rica for fruitful discussions.

APPENDIX

1. Derivation of the kinetic equation (17)

Starting from Eq. (14), one obtains the following equation for the evolution of $\mathbf{n}(z) = (n_m(z))_m$

$$\partial_z n_m(z) = 2\gamma \sum_{p,q,s} \mathrm{Im}[W_{mpqs} J_{mpqs}(z)], \tag{A1}$$

where $J_{mpqs} = \langle a_m^* a_p a_q^* a_s \rangle$ denotes the fourth-order moment. The equation governing the evolution of J_{mpqs} depends on the corresponding sixth-order moment. In this way one obtains an infinite hierarchy of moment equations, in which the nth order moment depends on the $n+2$-order moment. The closure of the hierarchy can be achieved following the random phase approximation [22]. Assuming that $|U/E| \ll 1$, linear dispersive effects dominate the interaction and bring the field close to Gaussian statistics [20]. By virtue of the factorizability property of statistical Gaussian fields, the sixth-order moment in the equation for J_{mpqs} can be factorized as a product of second-order moments. We obtain in this way

$$\partial_z J_{mpqs}(z) = i\Delta_{mpqs} J_{mpqs}(z) + 2i\gamma W^*_{mpqs} M_{mpqs}(\mathbf{n}(z)) + 2i\gamma R_{mpqs}(\mathbf{n}(z)), \tag{A2}$$

with

$$\Delta_{mpqs} = \beta_m + \beta_q - \beta_p - \beta_s, \tag{A3}$$

$$M_{mpqs}(\mathbf{n}) = n_m n_p n_q n_s \left(n_m^{-1} + n_q^{-1} - n_p^{-1} - n_s^{-1}\right), \tag{A4}$$

$$\begin{aligned} R_{mpqs}(\mathbf{n}) &= \delta^K_{q,s} U_{pm}(\mathbf{n})(n_p - n_m) n_q + \delta^K_{q,p} U_{sm}(\mathbf{n})(n_s - n_m) n_p \\ &\quad + \delta^K_{m,s} U_{pq}(\mathbf{n})(n_p - n_q) n_s + \delta^K_{m,p} U_{sq}(\mathbf{n})(n_s - n_q) n_m, \end{aligned} \tag{A5}$$

$$U_{pq}(\mathbf{n}) = \sum_s W_{pqss} n_s = \int u_p^*(\boldsymbol{r}) u_q(\boldsymbol{r}) \sum_s n_s |u_s(\boldsymbol{r})|^2 d\boldsymbol{r}, \tag{A6}$$

where $\delta^K_{q,s}$ denotes the Kronecker symbol $\delta^K_{q,s} = 1$ if the mode index $\{q\}$ equals $\{s\}$, $\delta^K_{q,s} = 0$ otherwise. We recall here that $\{q\}$ labels the two numbers (q_x, q_y) that specify the eigenmode $u_{q_x,q_y}(\boldsymbol{r})$ and its eigenvalue β_{q_x,q_y}.

We integrate the equation for J_{mpqs}

$$J_{mpqs}(z) = e^{i\Delta_{mpqs} z} J_{mpqs}(0) + 2i\gamma \int_0^z e^{i\Delta_{mpqs}(z-\zeta)} [W^*_{mpqs} M_{mpqs}(\mathbf{n}(\zeta)) + R_{mpqs}(\mathbf{n}(\zeta))] d\zeta,$$

and substitute into the equation for $\mathbf{n}$

$$\begin{aligned} \partial_z n_m(z) &= 2\gamma \sum_{p,q,s} \mathrm{Im}[e^{i\Delta_{mpqs} z} W_{mpqs} J_{mpqs}(0)] + 4\gamma^2 \sum_{p,q,s} \int_0^z d\zeta \cos[\Delta_{mpqs}(z-\zeta)] \{\mathrm{Re}[W_{mpqs} R_{mpqs}(\mathbf{n}(\zeta))] \\ &\quad + |W_{mpqs}|^2 M_{mpqs}(\mathbf{n}(\zeta))\} - 4\gamma^2 \sum_{p,q,s} \int_0^z d\zeta \sin[\Delta_{mpqs}(z-\zeta)] \mathrm{Im}[W_{mpqs} R_{mpqs}(\mathbf{n}(\zeta))]. \end{aligned}$$

Under the assumption $V_0/\beta_0 \gg 1$, we can take the continuum limit. If we denote $\tilde{n}_{\boldsymbol{k}}(z) = n_{[\boldsymbol{k}/\beta_0]}(z)$, then

$$\begin{aligned}\partial_z \tilde{n}_{\boldsymbol{\kappa}}(z) = {} & \frac{2\gamma}{\beta_0^6}\iiint d\boldsymbol{\kappa}_1 d\boldsymbol{\kappa}_2 d\boldsymbol{\kappa}_3 \mathrm{Im}\left[e^{i\tilde{\Delta}_{\boldsymbol{\kappa}\boldsymbol{\kappa}_1\boldsymbol{\kappa}_2\boldsymbol{\kappa}_3} z}\tilde{W}_{\boldsymbol{\kappa}\boldsymbol{\kappa}_1\boldsymbol{\kappa}_2\boldsymbol{\kappa}_3}\tilde{J}_{\boldsymbol{\kappa}\boldsymbol{\kappa}_1\boldsymbol{\kappa}_2\boldsymbol{\kappa}_3}(0)\right] + \frac{4\gamma^2}{\beta_0^6}\iiint d\boldsymbol{\kappa}_1 d\boldsymbol{\kappa}_2 d\boldsymbol{\kappa}_3 \int_0^z d\zeta \cos\left[\tilde{\Delta}_{\boldsymbol{\kappa}\boldsymbol{\kappa}_1\boldsymbol{\kappa}_2\boldsymbol{\kappa}_3}(z-\zeta)\right] \\ & \times \left\{\mathrm{Re}\left[\tilde{W}_{\boldsymbol{\kappa}\boldsymbol{\kappa}_1\boldsymbol{\kappa}_2\boldsymbol{\kappa}_3}\tilde{R}_{\boldsymbol{\kappa}\boldsymbol{\kappa}_1\boldsymbol{\kappa}_2\boldsymbol{\kappa}_3}(\tilde{\mathbf{n}}(\zeta))\right] + |\tilde{W}_{\boldsymbol{\kappa}\boldsymbol{\kappa}_1\boldsymbol{\kappa}_2\boldsymbol{\kappa}_3}|^2\tilde{M}_{\boldsymbol{\kappa}\boldsymbol{\kappa}_1\boldsymbol{\kappa}_2\boldsymbol{\kappa}_3}(\tilde{\mathbf{n}}(\zeta))\right\} \\ & - \frac{4\gamma^2}{\beta_0^6}\iiint d\boldsymbol{\kappa}_1 d\boldsymbol{\kappa}_2 d\boldsymbol{\kappa}_3 \int_0^z d\zeta \sin\left[\tilde{\Delta}_{\boldsymbol{\kappa}\boldsymbol{\kappa}_1\boldsymbol{\kappa}_2\boldsymbol{\kappa}_3}(z-\zeta)\right]\mathrm{Im}\left[\tilde{W}_{\boldsymbol{\kappa}\boldsymbol{\kappa}_1\boldsymbol{\kappa}_2\boldsymbol{\kappa}_3}\tilde{R}_{\boldsymbol{\kappa}\boldsymbol{\kappa}_1\boldsymbol{\kappa}_2\boldsymbol{\kappa}_3}(\tilde{\mathbf{n}}(\zeta))\right],\end{aligned}$$

where $\tilde{\beta}_{\boldsymbol{\kappa}} = \beta_{[\boldsymbol{\kappa}/\beta_0]}$, $\tilde{\Delta}_{\boldsymbol{\kappa}\boldsymbol{\kappa}_1\boldsymbol{\kappa}_2\boldsymbol{\kappa}_3} = \Delta_{[\boldsymbol{\kappa}/\beta_0][\boldsymbol{\kappa}_1/\beta_0][\boldsymbol{\kappa}_2/\beta_0][\boldsymbol{\kappa}_3/\beta_0]}$, and so on, $[x]$ being the integer part of x. The presence of the rapid phase allows us to use the following results:

$$\begin{aligned} m\iint_0^z \cos(m\Delta y)dy\phi(\Delta)d\Delta &= \int \mathrm{sinc}(v)\phi\left(\frac{v}{mz}\right)dv \overset{m\to\infty}{\longrightarrow} \pi\phi(0), \\ m\iint_0^z \sin(m\Delta y)dy\phi(\Delta)d\Delta &= 2\int \frac{\sin^2(v)}{v}\phi\left(\frac{2v}{mz}\right)dv \overset{m\to\infty}{\longrightarrow} 0,\end{aligned}$$

and we find

$$\partial_z\tilde{n}_{\boldsymbol{\kappa}}(z) = \frac{4\pi\gamma^2}{\beta_0^6}\iiint d\boldsymbol{\kappa}_1 d\boldsymbol{\kappa}_2 d\boldsymbol{\kappa}_3 \delta\left(\tilde{\Delta}_{\boldsymbol{\kappa}\boldsymbol{\kappa}_1\boldsymbol{\kappa}_2\boldsymbol{\kappa}_3}\right)\left\{\mathrm{Re}\left[\tilde{W}_{\boldsymbol{\kappa}\boldsymbol{\kappa}_1\boldsymbol{\kappa}_2\boldsymbol{\kappa}_3}\tilde{R}_{\boldsymbol{\kappa}\boldsymbol{\kappa}_1\boldsymbol{\kappa}_2\boldsymbol{\kappa}_3}(\tilde{\mathbf{n}}(z))\right] + \left|\tilde{W}_{\boldsymbol{\kappa}\boldsymbol{\kappa}_1\boldsymbol{\kappa}_2\boldsymbol{\kappa}_3}\right|^2\tilde{M}_{\boldsymbol{\kappa}\boldsymbol{\kappa}_1\boldsymbol{\kappa}_2\boldsymbol{\kappa}_3}(\tilde{\mathbf{n}}(z))\right\}.$$

We remark that the Kronecker symbol involved in $\tilde{R}_{\boldsymbol{\kappa}\boldsymbol{\kappa}_1\boldsymbol{\kappa}_2\boldsymbol{\kappa}_3}(\tilde{\mathbf{n}}(z))$ can be converted to a Dirac δ function $\delta^K_{[\boldsymbol{\kappa}_1/\beta_0],[\boldsymbol{\kappa}_2/\beta_0]} \to \beta_0^2\delta(\boldsymbol{\kappa}_1 - \boldsymbol{\kappa}_2)$. The contribution of the first term of $\tilde{R}_{\boldsymbol{\kappa}\boldsymbol{\kappa}_1\boldsymbol{\kappa}_2\boldsymbol{\kappa}_3}(\tilde{\mathbf{n}}(z))$ can thus be written as

$$\begin{aligned} I_1 &= \iiint d\boldsymbol{\kappa}_1 d\boldsymbol{\kappa}_2 d\boldsymbol{\kappa}_3 \delta\left(\tilde{\Delta}_{\boldsymbol{\kappa}\boldsymbol{\kappa}_1\boldsymbol{\kappa}_2\boldsymbol{\kappa}_3}\right)\mathrm{Re}\left[\tilde{W}_{\boldsymbol{\kappa}\boldsymbol{\kappa}_1\boldsymbol{\kappa}_2\boldsymbol{\kappa}_3}\delta^K_{[\boldsymbol{\kappa}_2/\beta_0],[\boldsymbol{\kappa}_3/\beta_0]}U_{[\boldsymbol{\kappa}_1/\beta_0][\boldsymbol{\kappa}/\beta_0]}(\mathbf{n})\left(n_{[\boldsymbol{\kappa}_1/\beta_0]} - n_{[\boldsymbol{\kappa}/\beta_0]}\right)n_{[\boldsymbol{\kappa}_2/\beta_0]}\right] \\ &= \beta_0^2\int d\boldsymbol{\kappa}_1\delta\left(\tilde{\beta}_{\boldsymbol{\kappa}_1} - \tilde{\beta}_{\boldsymbol{\kappa}}\right)\mathrm{Re}\left[\left(\int d\boldsymbol{\kappa}_2\tilde{W}_{\boldsymbol{\kappa}\boldsymbol{\kappa}_1\boldsymbol{\kappa}_2\boldsymbol{\kappa}_2}n_{[\boldsymbol{\kappa}_2/\beta_0]}\right)U_{[\boldsymbol{\kappa}_1/\beta_0][\boldsymbol{\kappa}/\beta_0]}(\mathbf{n})\left(n_{[\boldsymbol{\kappa}_1/\beta_0]} - n_{[\boldsymbol{\kappa}/\beta_0]}\right)\right] \\ &= \beta_0^4\int d\boldsymbol{\kappa}_1\delta\left(\tilde{\beta}_{\boldsymbol{\kappa}_1} - \tilde{\beta}_{\boldsymbol{\kappa}}\right)|U_{[\boldsymbol{\kappa}_1/\beta_0][\boldsymbol{\kappa}/\beta_0]}(\mathbf{n})|^2\left(n_{[\boldsymbol{\kappa}_1/\beta_0]} - n_{[\boldsymbol{\kappa}/\beta_0]}\right).\end{aligned}$$

We also made use of the fact that $U_{[\boldsymbol{\kappa}_1/\beta_0][\boldsymbol{\kappa}/\beta_0]}(\mathbf{n}) = \tilde{U}_{\boldsymbol{\kappa}_1\boldsymbol{\kappa}}(\tilde{\mathbf{n}}) = \frac{1}{\beta_0^2}\int d\boldsymbol{\kappa}'\tilde{W}_{\boldsymbol{\kappa}_1\boldsymbol{\kappa}\boldsymbol{\kappa}'\boldsymbol{\kappa}'}\tilde{n}_{\boldsymbol{\kappa}'}$, and $\tilde{U}_{\boldsymbol{\kappa}_1\boldsymbol{\kappa}}(\tilde{\mathbf{n}}) = \tilde{U}^*_{\boldsymbol{\kappa}\boldsymbol{\kappa}_1}(\tilde{\mathbf{n}})$. Proceeding similarly for the second term of $\tilde{R}_{\boldsymbol{\kappa}\boldsymbol{\kappa}_1\boldsymbol{\kappa}_2\boldsymbol{\kappa}_3}(\tilde{\mathbf{n}}(z))$, one obtains $I_1 = I_2$. The contributions of the third and fourth terms of $\tilde{R}_{\boldsymbol{\kappa}\boldsymbol{\kappa}_1\boldsymbol{\kappa}_2\boldsymbol{\kappa}_3}(\tilde{\mathbf{n}}(z))$ lead to

$$I_3 = I_4 = \beta_0^4\int d\boldsymbol{\kappa}_1 d\boldsymbol{\kappa}_2\delta\left(\tilde{\beta}_{\boldsymbol{\kappa}_1} - \tilde{\beta}_{\boldsymbol{\kappa}_2}\right)\mathrm{Re}\left[\tilde{W}_{\boldsymbol{\kappa}\boldsymbol{\kappa}\boldsymbol{\kappa}_2\boldsymbol{\kappa}_1}\tilde{U}_{\boldsymbol{\kappa}_1\boldsymbol{\kappa}_2}(\mathbf{n})\left(\tilde{n}_{\boldsymbol{\kappa}_1} - \tilde{n}_{\boldsymbol{\kappa}_2}\right)\tilde{n}_{\boldsymbol{\kappa}}\right].$$

A permutation of the variables $\boldsymbol{\kappa}_1$ and $\boldsymbol{\kappa}_2$ in this expression readily gives $I_3 = I_4 = 0$. Collecting all terms, we finally obtain the irreversible kinetic Eq. (17) governing the evolution of $\tilde{n}_{\boldsymbol{\kappa}}(z)$.

2. Homogeneous case $V(r) = 0$: usual WT kinetic equation

We show that the kinetic Eq. (17) recovers the conventional wave turbulence equation when the field is expanded in the usual plane-wave basis with periodic boundary conditions

$$u_{m_x,m_y}(\boldsymbol{r}) = \frac{1}{L}\exp[2i\pi(m_x x + m_y y)/L],$$

where L is the box size. This expansion is relevant to the homogeneous problem, that is, in the absence of the confining potential [$V(\mathbf{r}) = 0$ in the NLS Eq. (3)]. In this case the tensor W_{mpqs} recovers the following Kronecker $W_{mpqs} = \frac{1}{L^2}\delta^K_{m+q,p+s}$, so that the tensor $R_{mpqs}(\mathbf{n}(z))$ vanishes identically in Eq. (A2). It proves convenient here to make use of the conventional wave vector defined by $\boldsymbol{k} = \frac{2\pi}{L}(m_x, m_y) = \boldsymbol{\kappa}L/(2\pi\alpha)$, where we recall that $\boldsymbol{\kappa} = \beta_0(m_x, m_y)$, $\beta_{m_x,m_y} = \alpha(2\pi)^2(m_x^2 + m_y^2)/L^2 = \alpha k^2$ and $\beta_0 = \alpha(2\pi/L)^2$. In the continuum limit, the tensor W_{mpqs} then recovers the familiar Dirac δ function $|\tilde{W}_{\boldsymbol{\kappa}\boldsymbol{\kappa}_1\boldsymbol{\kappa}_2\boldsymbol{\kappa}_3}|^2 = \alpha^2\frac{(2\pi)^4}{L^8}\delta(\boldsymbol{\kappa}_1 + \boldsymbol{\kappa}_3 - \boldsymbol{\kappa}_2 - \boldsymbol{\kappa}) = \frac{(2\pi)^2}{L^6}\delta(\boldsymbol{k}_1 + \boldsymbol{k}_3 - \boldsymbol{k}_2 - \boldsymbol{k})$. Because of this Dirac δ function, the second term in the kinetic Eq. (17) vanishes, which thus leads to the usual wave turbulence kinetic equation [20–22]

$$\begin{aligned}\partial_z\tilde{n}_{\boldsymbol{k}}(z) = {} & \frac{4\pi\gamma^2}{(2\pi)^2}\iiint d\boldsymbol{k}_1 d\boldsymbol{k}_2 d\boldsymbol{k}_3\delta\left(\alpha\left(k_1^2 + k_3^2 - k_2^2 - k^2\right)\right) \\ & \times\delta(\boldsymbol{k}_1 + \boldsymbol{k}_3 - \boldsymbol{k}_2 - \boldsymbol{k})\mathcal{N}(\tilde{\mathbf{n}}),\end{aligned}$$

with

$$\mathcal{N}(\tilde{\mathbf{n}}) = \tilde{n}_{\boldsymbol{k}}\tilde{n}_{\boldsymbol{k}_1}\tilde{n}_{\boldsymbol{k}_2}\tilde{n}_{\boldsymbol{k}_3}\left(\tilde{n}_{\boldsymbol{k}}^{-1} + \tilde{n}_{\boldsymbol{k}_2}^{-1} - \tilde{n}_{\boldsymbol{k}_1}^{-1} - \tilde{n}_{\boldsymbol{k}_3}^{-1}\right).$$

Owing to the Dirac δ function over the momenta $\boldsymbol{k}$, this kinetic equation also conserves the total momentum $\mathbf{P} = \int \boldsymbol{k}\,\tilde{n}_{\boldsymbol{k}}\,d\boldsymbol{k}$.

3. Application to other waveguide configurations

The kinetic Eq. (17) is general and can be applied to different waveguide geometries or index profiles. We briefly

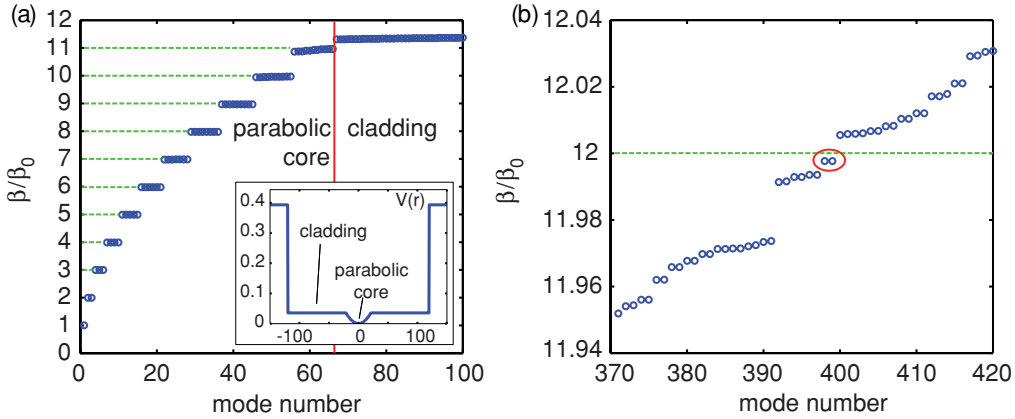

FIG. 5. (Color online) Representation of the eigenvalues (energies) of the modes of the system as a function of the mode number. (a) Modes of the parabolic core and the first few modes of the cladding. The inset depicts the potential $V(r)$ including the parabolic core and the cladding of respective radii $a = 21\ \mu$m and $a^{\rm cl} = 120\ \mu$m. (b) Eigenvalues of the modes of the cladding for an energy close to $\beta^{\rm cl} = 12 \times \beta_0$. The two circled modes can resonate with those modes in the core that verify the condition (A7), i.e., $\beta_{m_{11}} + \beta_{m_{11}} = \beta_{m_{10}} + \beta^{\rm cl}$.

illustrate this by considering the example of a circular waveguide of radius R whose index of refraction is supposed to be constant for $r < R$ ("step-index" waveguide). Moreover, we assume the waveguide to be of infinite depth for simplicity. The field can be expanded into the orthonormal basis of the Bessel functions $\psi(\boldsymbol{r},z) = \sum_{l,s} c_{l,s}(z) u_{l,s}(\boldsymbol{r}) \exp(-i\beta_{l,s} z)$, with

$$u_{l,s}(\boldsymbol{r}) = \frac{1}{\sqrt{\pi R^2 J_{l+1}^2(x_{l,s})}} J_l(x_{l,s} r/R) \exp(il\theta),$$

where $J_l(x)$ is the Bessel function of the first kind, $x_{l,s}$ is the sth zero of $J_l(x)$, and (r,θ) are the polar coordinates. With these notations, the eigenvalues read $\beta_{l,s} = \alpha x_{l,s}^2/R^2$. In a similar way as above, the passage to the continuum limit can be done by defining the wave vector $\boldsymbol{\kappa} = \beta_{0,1}(l,s)$, which thus leads to the kinetic equation for the evolution of $\tilde{n}_{\boldsymbol{\kappa}}(z)$. Note that with this parametrization of the wave vectors $\boldsymbol{\kappa}$ the density of states $\rho(\beta)$ is uniform.

4. Physical origin of the frequency cutoff

The existence of a frequency cutoff for the classical nonlinear wave finds its origin in the fact that modes whose eigenvalues exceed V_0 are not guided during the propagation. One may object, however, that this does not prevent a possible loss of power N due to the nonlinear excitation of modes with eigenvalues $\beta^{\rm cl} > V_0$ (i.e., modes in the cladding of the multimode fiber). In this Appendix we show that the efficiency of the generation of such modes is several orders of magnitude smaller than the conversion efficiency between guided modes, so that their excitations can be neglected. This provides a physical signification to the frequency cutoff discussed in this article.

According to the kinetic Eq. (17), new modes can be generated provided that they verify the condition of energy conservation given by the term $\delta(\tilde{\beta}_{\kappa_1} + \tilde{\beta}_{\kappa_3} - \tilde{\beta}_{\kappa_2} - \tilde{\beta}_{\kappa})$. The efficiency of the generation of such modes is determined by the corresponding mode overlap, $|\tilde{W}_{\kappa\kappa_1\kappa_2\kappa_3}|^2$. We first consider the case in which all modes in the core have been excited and we assess the efficiency of the generation of a single mode in the cladding. For this purpose, we model the cladding by a step-index waveguide whose radius $a^{\rm cl}$ is supposed much larger than the corresponding radius of the core, $a^{\rm cl} \gg a$. The respective potential $V(\mathbf{r})$ is depicted in the inset of Fig. 5(a). Figure 5(a) represents the eigenvalues of the modes of the system normalized to β_0 for the potential $V(\mathbf{r})$. Note that all the modes have not been reported here. We only report the modes of the parabolic core and the first 30 modes of the cladding, while Fig. 5(b) reports those modes of the cladding that resonate with the higher-order modes of the core (see the caption of Fig. 5). Also note that higher-order modes of the parabolic potential "feel" the presence of the cladding, and the corresponding eigenvalues slightly deviate from the analytical expression relevant to the infinite parabolic potential.

In the following we denote by β_{m_p} the eigenvalues of the modes in the core, where $\{m_p\}$ labels the two numbers (m_x,m_y) verifying $m_x + m_y + 1 = p$. The conservation of energy then reads

$$\beta_{m_{p_1}} + \beta_{m_{p_2}} = \beta_{m_{p_3}} + \beta^{\rm cl}. \tag{A7}$$

As illustrated in Fig. 5(a), we have 11 distinct energy levels in the core. In a first approximation, we consider that only those modes with energies $\beta_{m_{11}} = 11 \times \beta_0$ and $\beta_{m_{10}} = 10 \times \beta_0$ can generate a mode of energy $\beta^{\rm cl} = 12 \times \beta_0$. This latter mode corresponds to the lower-energy mode in the cladding verifying the condition (A7), namely $\beta_{m_{11}} + \beta_{m_{11}} = \beta_{m_{10}} + \beta^{\rm cl}$.

We now compare the efficiency of the generation of this cladding mode with the corresponding efficiency of the generation of a mode in the core. The efficiency of generation of a mode in the parabolic core is calculated by assuming that all modes with $p \leqslant 10$ have been excited. We thus calculate the efficiency of generation of a single mode with eigenvalue $\beta_{m_{11}}$ verifying the condition $\beta_{m_{10}} + \beta_{m_{10}} = \beta_{m_9} + \beta_{m_{11}}$. For this purpose, we calculate the coefficients $\mathcal{W}^{\rm cl}$ and $\mathcal{W}^{\rm co}$ defined as follows

$$\mathcal{W}^{\rm cl} = \frac{1}{\mathcal{N}^{\rm cl}} \sum_{\{m_{10}\}} \sum_{\{m_{11}\}} \sum_{\{m_{11}\}} \sum_{\{m^{\rm cl}\}} \left| W_{m_{10},m_{11},m_{11},m^{\rm cl}} \right|^2, \tag{A8}$$

$$\mathcal{W}^{\mathrm{co}} = \frac{1}{\mathcal{N}_{11}} \sum_{\{m_9\}} \sum_{\{m_{10}\}} \sum_{\{m_{10}\}} \sum_{\{m_{11}\}} \left| W_{m_9,m_{10},m_{10},m_{11}} \right|^2, \quad \text{(A9)}$$

where $\sum_{\{m_j\}}$ denotes a sum over all modes with the eigenvalue β_{m_j} ($j = 9,10,11$). Note that, to compare these two quantities, we normalized the calculation by the corresponding degeneracies of the energies β_{11} and β^{cl} (i.e., $\mathcal{N}_{11} = 11$ and $\mathcal{N}^{\mathrm{cl}} = 2$ denote the number of modes of energies $\beta_{m_{11}} = 11 \times \beta_0$ and $\beta^{\mathrm{cl}} = 12 \times \beta_0$). The computation of the sums (A8) and (A9) provides the following values

$$\frac{\mathcal{W}^{\mathrm{cl}}}{\mathcal{W}^{\mathrm{co}}} = \frac{6.4 \times 10^{-11}}{1.9 \times 10^{-5}} \sim 10^{-6}. \quad \text{(A10)}$$

Accordingly, *the generation of a mode in the cladding is six orders of magnitude less efficient than the corresponding efficiency of generation of a mode in the core*. This significant difference stems from the poor spatial overlap between a mode in the parabolic core and a mode in the cladding.

[1] M. Mitchell, Z. Chen, M. F. Shih, and M. Segev, Phys. Rev. Lett. **77**, 490 (1996).

[2] In noninstantaneous response nonlinear media, see, e.g., D. N. Christodoulides, T. H. Coskun, M. Mitchell, and M. Segev, Phys. Rev. Lett. **78**, 646 (1997); M. Mitchell, M. Segev, T. H. Coskun, and D. N. Christodoulides, *ibid.* **79**, 4990 (1997); D. N. Christodoulides, T. H. Coskun, M. Mitchell, Z. Chen, and M. Segev, *ibid.* **80**, 5113 (1998); Z. Chen *et al.*, Science **280**, 889 (1998); O. Bang, D. Edmundson, and W. Krolikowski, Phys. Rev. Lett. **83**, 5479 (1999); M. Peccianti and G. Assanto, Opt. Lett. **26**, 1791 (2001); B. Hall, M. Lisak, D. Anderson, R. Fedele, and V. E. Semenov, Phys. Rev. E **65**, 035602 (2002).

[3] A. Hasegawa, Opt. Lett. **5**, 416 (1980).

[4] In instantaneous response nonlinear media, see, e.g., A. Picozzi and M. Haelterman, Phys. Rev. Lett. **86**, 2010 (2001); A. Picozzi, C. Montes, and M. Haelterman, Phys. Rev. E **66**, 056605 (2002); A. Picozzi, M. Haelterman, S. Pitois, and G. Millot, Phys. Rev. Lett. **92**, 143906 (2004); A. Sauter, S. Pitois, G. Millot, and A. Picozzi, Opt. Lett. **30**, 2143 (2005); M. Wu, P. Krivosik, B. A. Kalinikos, and C. E. Patton, Phys. Rev. Lett. **96**, 227202 (2006); C. Rotschild *et al.*, Nature Photon. **2**, 371 (2008); B. Alfassi, C. Rotschild, and M. Segev, Phys. Rev. A **80**, 041808 (2009).

[5] A. Hasegawa, Phys. Fluids **18**, 77 (1975); **20**, 2155 (1977).

[6] B. Barviau, S. Randoux, and P. Suret, Opt. Lett. **31**, 1696 (2006); A. Picozzi and M. Haelterman, Phys. Rev. Lett. **92**, 103901 (2004); D. V. Dylov and J. W. Fleischer, *ibid.* **100**, 103903 (2008); A. Picozzi, S. Pitois, and G. Millot, *ibid.* **101**, 093901 (2008); A. Fratalocchi, C. Conti, G. Ruocco, and S. Trillo, *ibid.* **101**, 044101 (2008); J. Garnier and A. Picozzi, Phys. Rev. A **81**, 033831 (2010).

[7] A. Picozzi and P. Aschieri, Phys. Rev. E **72**, 046606 (2005); S. Pitois, S. Lagrange, H. R. Jauslin, and A. Picozzi, Phys. Rev. Lett. **97**, 033902 (2006); B. Barviau, B. Kibler, S. Coen, and A. Picozzi, Opt. Lett. **33**, 2833 (2008); B. Barviau, B. Kibler, A. Kudlinski, A. Mussot, G. Millot, and A. Picozzi, Opt. Express **17**, 7392 (2009); B. Barviau, B. Kibler, and A. Picozzi, Phys. Rev. A **79**, 063840 (2009); L. Levi *et al.*, Opt. Express **16**, 7818 (2008); S. Lagrange, H. R. Jauslin, and A. Picozzi, Europhysics Lett. **79**, 64001 (2007); A. Picozzi, Opt. Express **16**, 17171 (2008); A. Picozzi and S. Rica, Europhys. Lett. **84**, 34004 (2008); P. Suret, S. Randoux, H. R. Jauslin, and A. Picozzi, Phys. Rev. Lett. **104**, 054101 (2010); C. Michel, P. Suret, S. Randoux, H. R. Jauslin, and A. Picozzi, Opt. Lett. **35**, 2367 (2010); D. B. Soh *et al.*, Opt. Express **18**, 22393 (2010).

[8] A. Picozzi, Opt. Express **15**, 9063 (2007).

[9] U. Bortolozzo, J. Laurie, S. Nazarenko, and S. Residori, J. Opt. Soc. Am. B **26**, 2280 (2009).

[10] Y. Silberberg, Y. Lahini, Y. Bromberg, E. Small, and R. Morandotti, Phys. Rev. Lett. **102**, 233904 (2009).

[11] C. Barsi, W. Wan, and J. W. Fleischer, Nature Photon. **3**, 211 (2009).

[12] C. Conti, M. Leonetti, A. Fratalocchi, L. Angelani, and G. Ruocco, Phys. Rev. Lett. **101**, 143901 (2008).

[13] R. Weill, B. Fischer, and O. Gat, Phys. Rev. Lett. **104**, 173901 (2010); R. Weill, B. Levit, A. Bekker, O. Gat, and B. Fischer, Opt. Express **18**, 16520 (2010).

[14] E. G. Turitsyna, G. Falkovich, V. K. Mezentsev, and S. K. Turitsyn, Phys. Rev. A **80**, 031804 (2009).

[15] S. Babin, D. Churkin, A. Ismagulov, S. Kablukov, and E. Podivilov, J. Opt. Soc. Am. B **24**, 1729 (2007); S. A. Babin, V. Karalekas, E. Podivilov, V. K. Mezentsev, P. Harper, J. D. Ania-Castanon, and S. K. Turitsyn, Phys. Rev. A **77**, 033803 (2008); S. Babin *et al.*, Opt. Lett. **33**, 633 (2008).

[16] S. K. Turitsyn *et al.*, Nature Photon. **4**, 231 (2010); D. V. Churkin, S. A. Babin, A. E. El-Taher, P. Harper, S. I. Kablukov, V. Karalekas, J. D. Ania-Castanon, E. V. Podivilov, and S. K. Turitsyn, Phys. Rev. A **82**, 033828 (2010).

[17] J. Klaers, F. Vewinger, and M. Weitz, Nature Phys. **6**, 512 (2010); J. Klaers *et al.*, Nature (London) **468**, 545 (2010).

[18] Y. Bromberg, Y. Lahini, E. Small, and Y. Silberberg, Nature Photon. **4**, 721 (2010).

[19] C. Sun, S. Jia, C. Barsi, S. Rica, A. Picozzi, and J. W. Fleischer (unpublished).

[20] D. J. Benney and P. G. Saffman, Proc. R. Soc. London A **289**, 301 (1966); A. C. Newell, Rev. Geophys. **6**, 1 (1968); A. C. Newell, S. Nazarenko, and L. Biven, Physica D **152**, 520 (2001); Y. Choi, Y. V. Lvov, and S. Nazarenko, *ibid.* **201**, 121 (2005).

[21] V. N. Tsytovich, *Nonlinear Effects in Plasma* (Plenum, New York, 1970); A. Hasegawa, *Plasma Instabilities and Nonlinear Effects* (Springer-Verlag, Berlin, 1975).

[22] V. E. Zakharov, V. S. L'vov, and G. Falkovich, *Kolmogorov Spectra of Turbulence I* (Springer, Berlin, 1992); V. E. Zakharov, F. Dias, and A. Pushkarev, Phys. Rep. **398**, 1 (2004).

[23] S. Dyachenko *et al.*, Physica D **57**, 96 (1992); Y. Pomeau, *ibid.* **61**, 227 (1992); V. E. Zakharov and S. V. Nazarenko, *ibid.* **201**, 203 (2005).

[24] C. Connaughton, C. Josserand, A. Picozzi, Y. Pomeau, and S. Rica, Phys. Rev. Lett. **95**, 263901 (2005).

[25] N. G. Berloff and B. V. Svistunov, Phys. Rev. A **66**, 013603 (2002).

[26] G. Düring, A. Picozzi, and S. Rica, Physica D **238**, 1524 (2009).

[27] M. J. Davis, S. A. Morgan, and K. Burnett, Phys. Rev. Lett. **87**, 160402 (2001); Phys. Rev. A **66**, 053618 (2002); P. B. Blakie and M. J. Davis, *ibid.* **72**, 063608 (2005); M. J. Davis and P. B. Blakie, Phys. Rev. Lett. **96**, 060404 (2006).

[28] Y. S. Kivshar and G. P. Agrawal, *Optical Solitons: From Fibers to Photonic Crystals* (Academic Press, San Diego, 2003).

[29] L. Pitaevskii and S. Stringari, *Bose-Einstein Condensation* (Oxford University Press, New York, 2003).

[30] A. Yariv, *Optical Electronics*, 4th ed. (Saunders College Publishing, Philadelphia, PA, 1991).

[31] Note that a different approach, combining the Wentzel-Kramers-Brillouin (WKB) description of inhomogeneous waves and the WT theory has been proposed in Y. Lvov, S. Nazarenko, and R. West, Physica D **184**, 333 (2003). A kinetic equation is derived in which the nontrivial element appears through the linear WKB dynamics, whereas modifications of the nonlinear collision integral are fairly straightforward.

[32] In the Karhunen-Loeve expansion, $\{u_m(\boldsymbol{r})\}$ are eigenfunctions of the integral equation $\int B(\boldsymbol{r}_1,\boldsymbol{r}_2)u_m(\boldsymbol{r}_2)d\boldsymbol{r}_2 = n_m u_m(\boldsymbol{r}_1)$, where n_m are the corresponding eigenvalues and $B(\boldsymbol{r}_1,\boldsymbol{r}_2,z) = \langle\psi(\boldsymbol{r}_1,z)\psi^*(\boldsymbol{r}_2,z)\rangle$ is the correlation function. The modal expansion of the correlation function reads $B(\boldsymbol{r}_1,\boldsymbol{r}_2) = \sum_m n_m u_m(\boldsymbol{r}_1)u_m^*(\boldsymbol{r}_2)$. In the quantum context, the correlation function is known as the one-body density matrix, which allows one to define the concept of long-range order [see, e.g., Chap. 2 in A. J. Leggett, *Quantum Liquids* (Oxford University Press, New York, 2006), or Chap. 1 in L. Pitaevskii, and S. Stringari, *Bose-Einstein Condensation* (Oxford University Press, New York, 2003)].

[33] A. J. Leggett, *Quantum Liquids* (Oxford University Press, New York, 2006).

[34] B. Rumpf and A. C. Newell, Phys. Rev. Lett. **87**, 054102 (2001); Physica D **184**, 162 (2003); B. Rumpf, Phys. Rev. E **69**, 016618 (2004); K. Hammani, B. Kibler, C. Finot, and A. Picozzi, Phys. Lett. A **374**, 3585 (2010).

[35] G. I. Stegeman and R. H. Stolen, J. Opt. Soc. Am. B **6**, 652 (1989); A. E. Fomin, M. L. Gorodetsky, I. S. Grudinin, and V. S. Ilchenko, *ibid.* **22**, 459 (2005); D. Kouznetsov, J. Moloney, and E. M. Wright, *ibid.* **18**, 743 (2001).

[36] See, e.g., J. Billy *et al.*, Nature (London) **453**, 891 (2008); G. Roati *et al.*, *ibid.* **453**, 895 (2008); B. Deissler *et al.*, Nature Phys. **6**, 354 (2010); L. Sanchez-Palencia and M. Lewenstein, *ibid.* **6**, 87 (2010).

[37] See, e.g., V. Doya, O. Legrand, F. Mortessagne, and C. Miniatura, Phys. Rev. Lett. **88**, 014102 (2001); Phys. Rev. E **65**, 056223 (2002).

[38] E. J. Heller, Phys. Rev. Lett. **53**, 1515 (1984); H.-J. Stöckman, *Quantum Chaos: An Introduction* (Cambridge University Press, Cambridge, England, 1999).